Geophysical Research Letters

RESEARCH LETTER
10.1029/2024GL113595

Explaining Observed Daily Variations and Decadal Trends in the Diurnal Air Temperature Range

Sarosh Alam Ghausi[1,2], Kaighin McColl[3,4], Erwin Zehe[2], and Axel Kleidon[1]

[1]Biospheric Theory and Modelling Group, Max Planck Institute for Biogeochemistry, Jena, Germany, [2]Institute of Water Resources and River Basin Management, Karlsruhe Institute of Technology–KIT, Karlsruhe, Germany, [3]Department of Earth and Planetary Sciences, Harvard University, Cambridge, MA, USA, [4]School of Engineering and Applied Sciences, Harvard University, Cambridge, MA, USA

Key Points:

- Diurnal air temperature range (DTR) is primarily governed by the heat storage changes within the lower atmosphere due to solar radiation
- DTR carries imprints of surface evaporative conditions and can be used to assess water stress from near-surface atmospheric observations
- Empirically observed multi-decadal decline in DTR can be reproduced by changes in the greenhouse gas forcings alone

Supporting Information:

Supporting Information may be found in the online version of this article.

Correspondence to:

S. A. Ghausi,
sghausi@bgc-jena.mpg.de

Citation:

Ghausi, S. A., McColl, K., Zehe, E., & Kleidon, A. (2025). Explaining observed daily variations and decadal trends in the diurnal air temperature range. *Geophysical Research Letters*, *52*, e2024GL113595. https://doi.org/10.1029/2024GL113595

Received 9 NOV 2024
Accepted 8 JUL 2025

Author Contributions:

Conceptualization: Sarosh Alam Ghausi, Kaighin McColl, Erwin Zehe, Axel Kleidon
Formal analysis: Sarosh Alam Ghausi
Methodology: Sarosh Alam Ghausi, Axel Kleidon
Supervision: Kaighin McColl, Erwin Zehe, Axel Kleidon
Writing – original draft: Sarosh Alam Ghausi
Writing – review & editing: Kaighin McColl, Erwin Zehe, Axel Kleidon

Abstract Understanding variability and trends in the near-surface diurnal air temperature range (DTR) remains unclear due to its complex interactions with antecedent radiative and hydrologic conditions. Here, we use a thermodynamic systems approach, and show that DTR primarily reflects changes in lower atmospheric heat storage, governed by diurnally constrained non-latent energy input from the surface into the atmospheric boundary layer. This approach predicts DTR across a range of climates, reproduces its day-to-day variations, and explains its decline with rising greenhouse gas (GHG) concentrations. We show that in addition to strong controls exerted by radiation and cloud cover, DTR carries imprints of surface water stress during the water-limited evaporative regime. Our expression yields a mean reduction of 0.23°C in DTR per 1°C rise in temperatures, in response to changes in GHG forcings. Our findings imply that the first-order decline in DTR with global warming can be explained by increased GHG forcings alone.

Plain Language Summary The diurnal air temperature range (DTR, the difference between daily maximum and minimum air temperatures) impacts human health, ecosystems and food production. Long-term (multi-decadal) observations typically show that DTR declines with global warming. The physical reasoning behind this trend remains unclear as a result of the intricate dependence of DTR on multiple atmospheric and land-surface processes within the Earth system. Here, we present a physical theory for DTR that explains its day-to-day variations as well as its long-term decline with rising GHG concentrations. We derive an expression for DTR hypothesizing that it primarily reflects changes in energy stored in the lower atmosphere. Our approach then explains both short (daily) and long-term (multi-decadal) response of DTR to changes in clouds, surface-water availability and greenhouse gas radiative forcings. Our findings imply that the first-order observed decline in DTR can be reproduced by changes in GHG concentrations alone without accounting for other changes. Our expression can also be used to diagnose changes in DTR in response to aerosols, vegetation and other aspects of global change as well.

1. Introduction

The diurnal air-temperature range (DTR), defined as the difference between daily maximum and minimum air temperature, is one of the most important and well-observed climatological variables. It exerts a direct control on vegetation productivity, crop yield and human health (Lei et al., 2020; Lobell, 2007; J. Wang and Liu, 2023; Yang et al., 2013). Empirical analysis of observations has revealed an asymmetric warming between maximum and minimum air temperatures, leading to a decline in DTR since 1950 at the rate around −0.05°C decade $^{-1}$ (Easterling et al., 1997; Karl et al., 1991; Sun et al., 2018). This decline abated in some areas after the 1980s, coincident with solar brightening, while DTR continued to decline in other regions (Huang et al., 2023; Wild, 2005; Zhou et al., 2004). The precise reasons behind these changes remain unclear.

Changes in DTR over land are intricately linked to both atmospheric and land-surface processes through the surface energy balance. Atmospheric controls encompass changes in clouds, aerosols, circulation patterns and heat storage which modulates radiative heating at the surface and have been shown to partially control DTR (Betts et al., 2013; Bristow & Campbell, 1984; Dai et al., 1999; Doan et al., 2022; Huang et al., 2006; Makowski et al., 2009). Land surface controls include variations in soil moisture, albedo, and vegetation types. They modulate variations in DTR by affecting the vertical turbulent exchange of sensible and latent heat through changes in surface roughness, root water uptake and plant hydraulics (Mearns et al., 1995; Panwar et al., 2019; Panwar & Kleidon, 2022; Zhou et al., 2007). The coupling between land and atmosphere further buffer these

variations through changes in boundary layer dynamics (Doan et al., 2022). State-of-the-art climate models struggle to simulate these changes due to associated uncertainties in the representation of cloud cover and land-surface processes (Lewis & Karoly, 2013; Stone & Weaver, 2003; K. Wang & Clow, 2020). Different generations of climate models have consistently underestimated the decline in DTR relative to observations. This has been attributed to their limitations in capturing day-to-day dynamics and the stronger simulated increase in maximum temperatures (Braganza et al., 2004; Lewis & Karoly, 2013; K. Wang & Clow, 2020). Consequently, the underlying causal factors responsible for trends in DTR remain largely model dependent and it has been identified as a substantial knowledge gap in a recent IPCC report (IPCC, 2021; Stone & Weaver, 2003). While many processes contribute to DTR variability, it is unclear which processes are essential to explaining most of that variability. We require a hierarchy of models of varying complexity to truly understand DTR variability, just as we do for other aspects of climate (Held, 2005).

To address this gap, we follow a minimalist approach and use basic physical principles to derive an expression for DTR that explains its day-to-day variation as well as its long-term observed decline with global warming. We hypothesize that variations in DTR are primarily shaped by diurnally constrained energy input from the surface into the atmospheric boundary layer. This energy input essentially refers to the part of solar radiation that is not partitioned into evaporating water (Panwar et al., 2019). This includes sensible heating and heating of the lower atmosphere by net longwave radiation. Consequently, this suggests that, in addition to radiation and clouds, the availability of water at the surface will influence DTR by altering the Bowen ratio.

To show this, we use an energetically constrained box-model for the lower atmosphere and force it with observed radiative and evaporative conditions to estimate heat storage variations, which we then link to air temperature variations. In addition to the surface energy balance, we explicitly constrain the vertical turbulent exchange between the surface and the lower atmosphere using the thermodynamic limit of maximum power (Kleidon & Renner, 2013). This constraint arises in the form of the maximum work which can be performed to maintain vertical turbulent mixing in the atmosphere for a given radiative heating of the surface. This thermodynamic framework has already been tested against observations and has shown a remarkable ability to reproduce the observed diurnal and seasonal evolution of turbulent fluxes over land (Conte et al., 2019; Ghausi et al., 2023; Kleidon & Renner, 2013, 2018). This approach then enables us to derive an expression for DTR that solely relies on physical principles, observed incoming radiative fluxes and surface evaporative conditions.

The objectives of this study are threefold: firstly, we evaluate the performance of this approach against daily DTR observations from FLUXNET sites and the ERA5 reanalysis; secondly, we assess how changes in radiative forcing, cloud cover and surface-water availability modulate DTR via their impacts on energy storage in the lower atmosphere. Thirdly and finally, we estimate the first-order response of DTR to increases in greenhouse-gas radiative forcing and compare our theoretical prediction with multi-decadal trends in observations and climate-model simulations. These objectives provide the structural sub-headings used for the Results and Discussion section.

2. Model Conceptualization

We used a three-layered energy-budget framework that accounts for surface energy balance, changes in energy storage within the atmospheric boundary layer and thermodynamic constraint on vertical turbulent flux exchange. This is demonstrated in Figure 1a and further described in Supporting Information S1 (Text S1 and S2).

The net absorbed solar radiation and downwelling longwave radiation heats the surface, which then cools by emitting longwave radiation and exchanging turbulent fluxes of sensible and latent heat. In this model, all energy emitted from the surface eventually is emitted to space through outgoing longwave radiation ($R_{\mathrm{l,toa}}$). This, however, does not happen immediately and results in heat storage changes (dU/dt) within the lower atmosphere. We can then write the energy balance of the lower atmosphere as:

$$\frac{dU}{dt} = H_{\mathrm{in}} - H_{\mathrm{out}} \tag{1}$$

Here, H_{in} is the addition of energy into the lower atmosphere and is primarily determined by the part of absorbed solar radiation (R_{s}) which does not contribute to evaporating water (LE) at the surface ($H_{\mathrm{in}} = R_{\mathrm{s}} - \mathrm{LE}$). H_{out} represents the energy lost from the top of the atmosphere to space as outgoing longwave radiation and is described

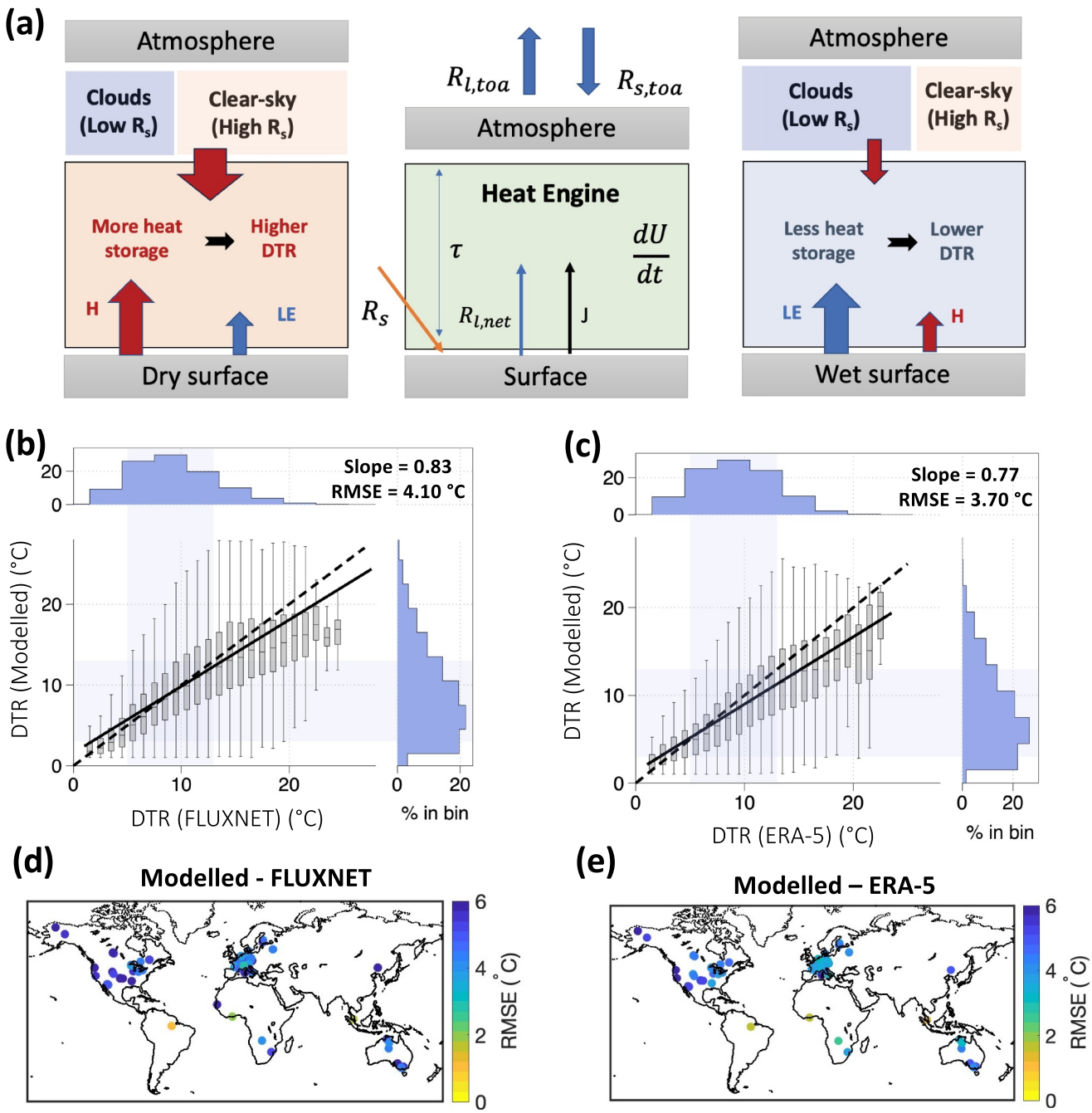

Figure 1. (a) Schematic diagram of the conceptualized surface-atmosphere system as a heat engine described by incoming solar radiation (R_s), net longwave radiation ($R_{l,net}$), changes in the lower atmosphere heat storage (dU/dt) and turbulent flux exchange (J = H + LE) of sensible (H) and latent heat (LE). Comparison of the daily values of estimated diurnal temperature range with (b) FLUXNET observations and (c) ERA5 reanalysis at the FLUXNET sites. The mid-horizontal line in the boxplots represents the median. The shaded box shows the interquartile range (IQR), spanning from the 25th percentile (Q1) to the 75th percentile (Q3). The whiskers are drawn to the smallest/largest non-outlier. Outliers are defined as either Q1 − 1.5 IQR or Q3 + 1.5 IQR. The solid black line corresponds to the regression fit line while dotted black line represent the 1:1 correspondance. The blue shaded regions denote the IQR for the frequency density of points (%/bin) (d) root mean squared error between estimated diurnal temperature and FLUXNET observations for each site. (e) same as (d) but between estimated and ERA5 data at each site.

using $R_{l,toa}$. For simplicity, ground heat flux is neglected as well as heating or cooling by horizontal transport. Our analysis is restricted to days with mean temperatures greater than 0°C, so we assume no heat loss through snow and ice-melting.

In addition to the energy balance, we impose an additional constraint on the vertical turbulent exchange. This is done by setting it to the value consistent with that of an atmosphere operating at the maximum power limit. Following the approach adopted in (Conte et al., 2019; Kleidon & Renner, 2018), the expression for the optimum turbulent flux can be described as:

$$J_{\text{opt}} = \frac{1}{2}\left(R_s + \left(\frac{3}{4}\tau - 1\right)R_{l,\text{toa}} + \frac{dU}{dt}\right) \tag{2}$$

here τ is the longwave optical thickness of the atmosphere, and dU/dt denotes heat storage changes. τ is calculated from the parameterization of downwelling longwave radiation as $R_{\text{ld}} = 3/4\ \tau\ R_{\text{l,toa}}$ (Conte et al., 2019; Kleidon & Renner, 2017), as described by the gray atmosphere radiative equilibrium solution (Dhara, 2017; Goody & Yung, 1989). This model is based on a gray atmosphere approximation where longwave optical thickness is integrated over the terrestrial spectrum although gas absorption is wavelength-dependent. The coefficient 3/4 comes from Eddington's approximation (Lorenz & McKay, 2003) and accounts for how much of the outgoing longwave radiation is re-emitted back to the Earth's surface.

We test the maximum power approach with this parameterization of downwelling longwave radiation and find good agreement when compared with observed turbulent fluxes over FLUXNET sites (Figure S2 in Supporting Information S1). The turbulent fluxes were slightly overestimated which is likely due to the assumption of no ground heat storage changes and not accounting for the atmospheric window effect in longwave radiative transfer (Conte et al., 2019; Dhara et al., 2016; Ghausi et al., 2023).

The daily evaporation averaged over 24 hr is defined as:

$$\text{LE} = f_w f_{\text{eq}} J_{\text{opt}} \tag{3}$$

here J_{opt} is the optimized turbulent flux obtained using Equation 2, f_{eq} is the equilibrium evaporative fraction (Priestley & Taylor, 1972; Slatyer & McIlroy, 1961) which was estimated as the ratio of latent heat flux (calculated using equilibrium partitioning of net radiation) to total turbulent fluxes (Text S2 in Supporting Information S1) and f_{w} is the water-availability factor which is calculated as the ratio of actual to equilibrium evaporation. Actual evaporation was obtained from the FLUXNET observations.

We then hypothesize that the diurnal variations in air temperature over land are dominated by the energy input from the land surface. The total energy accumulation during the day is then described as

$$\Delta U = \int_{\text{day}} \left(\frac{dU}{dt}\right) dt = \int_{\text{day}} (H + R_{l,\text{net}})\, dt = \int_{\text{day}} \left(R_s - f_w f_{\text{eq}} J_{\text{opt}}\right) dt \tag{4}$$

This energy input leads to changes in boundary layer heat storage. We assume that the boundary layer grows to a height of h as the air temperature increases during the day and changes in the diurnal amplitude of potential temperature are equal to the diurnal range of air temperature (Stull, 2017). The total change in the energy stored during the day within the boundary layer can then be expressed as (Panwar et al., 2019):

$$\Delta U = \int_{\text{day}} \left(\frac{dU}{dt}\right) = \frac{1}{2} c_p \rho h (T_{\max} - T_{\min}) \tag{5}$$

here c_{p} is the specific heat capacity of air (1,005 J $\text{kg}^{-1}\text{k}^{-1}$), ρ is the air density (1.23 kg m^{-3}), and h is the maximum growth in the boundary layer height reached during day, which was approximated here as $h = 1{,}000$ m (McColl et al., 2019). The coefficient ½ comes from the assumption that boundary layer height (h) grows linearly with increases in air temperature (Panwar et al., 2019; Panwar and Kleidon, 2022). This stored energy is eventually emitted to space resulting in a steady state over the diurnal cycle. The model assumes that there is no heat storage transfer from one day to the other and is applied to all the days when air temperatures exceed 0°C that may or may not be continuous. The model also does not explicitly account for nocturnal ground heat release, which can

affect minimum temperatures. Combining Equations 2, 4, and 5, yields an expression for DTR which solely relies on observed radiative forcings and surface evaporative conditions:

$$T_{\max} - T_{\min} = \mathrm{DTR} = \frac{2}{c_p \rho h} \cdot \left(\left(\frac{2 - f_w f_{\mathrm{eq}}}{2 + f_w f_{\mathrm{eq}}} \right) R_s - \frac{f_w f_{\mathrm{eq}}}{2 + f_w f_{\mathrm{eq}}} \left(\frac{3}{4} \tau - 1 \right) R_{l,\mathrm{toa}} \right) \Delta t \quad (6)$$

here Δt is the length of daytime (calculated as periods when $R_s > 5$ W/m^2) and τ is the longwave optical thickness of the atmosphere. Equation 6 is used to estimate DTR at daily time step using observed data from 82 flux tower sites. A worked example to implement this approach is described in Table S3 in Supporting Information S1.

3. Data Sets Used

The analysis was performed over 82 FLUXNET sites from FLUXNET-2015 data set (Pastorello et al., 2020). Seventy-four of these sites lie in the mid-latitudes (ranging from 23°N–66°N and 23°S–66°S). Further information on each site is summarized in Table S1 in Supporting Information S1. These sites provide half hourly observations of net shortwave and longwave radiation, sensible, latent and ground heat fluxes, and near surface air temperature. The daily mean fields (averaged over 24 hr) were used for the analysis. The FLUXNET data was gap filled using the multidimensional scaling (MDS) method (Reichstein et al., 2005). Only data with a "good" quality flag (quality flag <1) was used for the analysis, with further details described in Pastorello et al. (2020). Potential evaporation was derived using the equilibrium partitioning of net radiation (Priestley & Taylor, 1972; Slatyer & McIlroy, 1961) from FLUXNET data. Outgoing longwave radiation at top of atmosphere was derived from NASA-CERES data set (Kato et al., 2018; Loeb et al., 2018). In addition to FLUXNET sites, all the results were also evaluated against the ERA5 reanalysis data (Muñoz Sabater, 2019) interpolated over these sites. List of all the variables, their notations and data sources is also summarized in Table S2 in Supporting Information S1.

4. Results and Discussion

4.1. Evaluation of the Modeled DTR With Observations and ERA5

We start by evaluating the accuracy of our estimates using observations from 82 FLUXNET sites over ice-free land regions spanning a wide range of climates. Only sites with at least 2 years of continuous data for all the variables were used for the analysis (Table S1 in Supporting Information S1). We repeated the analysis using ERA5 reanalysis data interpolated over these sites. Our comparison showed that we were able to predict the day-to-day variations in DTR over these sites with a root mean squared error (RMSE) of 3–4°C (corresponding to a relative error of 15%–20%) with both FLUXNET and ERA5 (Figures 1b and 1c). These error values are only slightly larger than the differences in DTR, estimated by comparing the FLUXNET observations with ERA5 data (Figures S3 and S4 in Supporting Information S1). The spread in the regression plots were reduced when tropical and mid-latitude sites were separated (Figure S5 in Supporting Information S1). The global map showing RMSE values for each site with respect to FLUXNET and ERA5 data is shown in Figures 1d and 1e respectively. The evaluation was also performed globally using alternative data sets with global coverage, which produced qualitatively similar results (Text S5 and Figure S7 in Supporting Information S1). Although some distinct biases exist, our results demonstrate that our physical approach allows us to predict the daily variations in DTR as accurately as flux tower observations. Some of these biases are also attributable to the observational errors in latent heat flux (LE) from the FLUXNET data. This is illustrated by the difference between estimated DTRs when using direct LE observations compared to when LE is diagnosed using energy-balance closure, yielding an RMSE of 2°C (Figure S6 in Supporting Information S1). We also assessed the sensitivity of our modeled DTR to unaccounted processes, such as changes in ground heat flux and boundary layer height, and found that they can introduce differences in DTR of around 3–4°C; comparable to the RMSE between our model and observations (Text S6 and S7 in Supporting Information S1).

Next, we investigated how effectively our model captures the distinct responses of DTR to changes in radiative and land-surface conditions. To investigate this, we used the clear-sky fraction (f_c) defined as the ratio of daily incoming solar radiation at the surface to potential solar radiation at the top of atmosphere (Renner et al., 2019). High values of f_c (typically more than 0.6) indicate clear-sky conditions while lower values indicate cloudier conditions. We observed a monotonic first-order increase in the DTR with increase in clear-sky fraction indicating higher DTR with fewer clouds, in line with prior studies (Bristow & Campbell, 1984). These responses

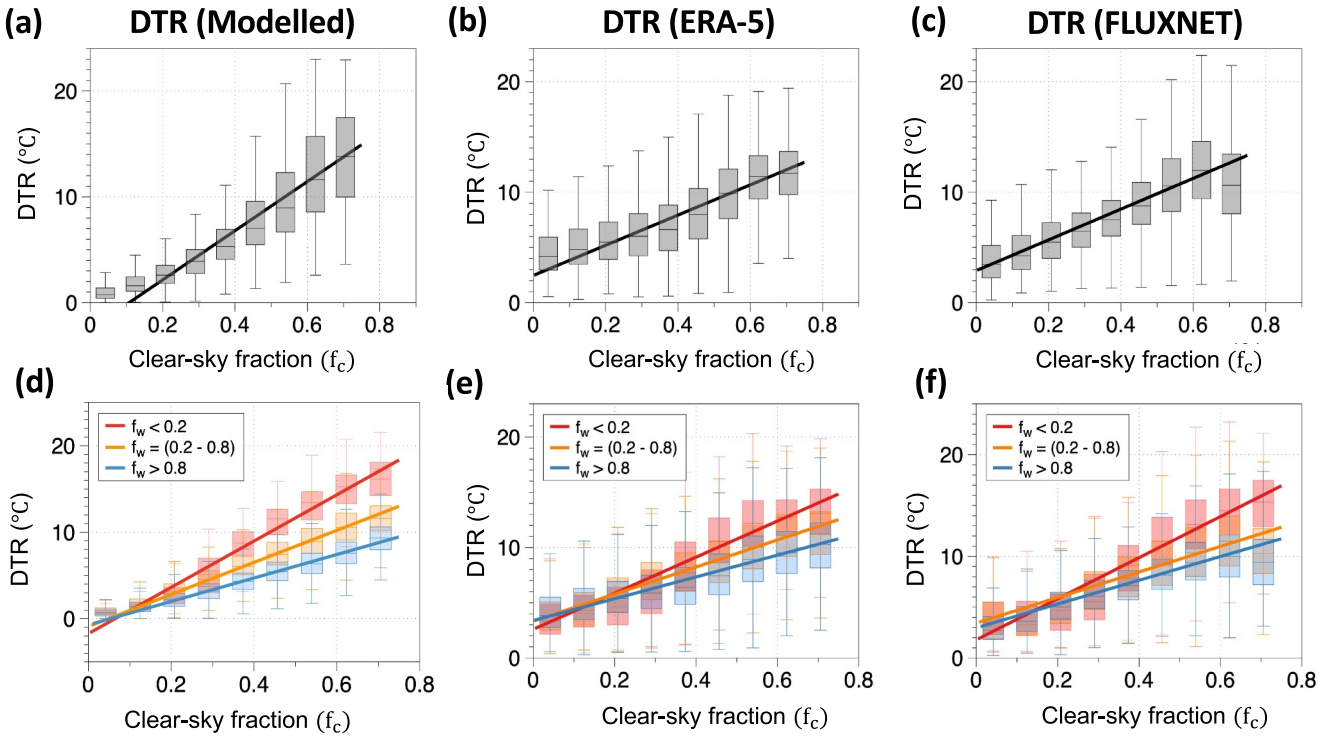

Figure 2. Variation of the diurnal air temperature range with clear-sky fraction (f_c, defined as the ratio of downward surface to potential solar radiation) for (a) estimated values, (b) ERA5, and (c) FLUXNET respectively. (d–f) same as (a–c) but stratified based on different surface water availability conditions (f_w, defined as the ratio of actual to potential evaporation). Boxplot elements are as described in Figure 1.

observed in FLUXNET and ERA5 data sets were very well reproduced by our approach (Figures 2a–2c). The slopes between the estimated DTR and f_c at each individual site also compared reasonably well with those obtained using FLUXNET and ERA5 data (Figure S9 in Supporting Information S1). The reduction in DTR with clouds primarily occurs due to two reasons: (a) reduced solar absorption due to clouds during the day that reduces the maximum day-time temperature; and (b) an increased longwave optical thickness of the atmosphere due to clouds that increases the night-time minimum temperatures. Our interpretation is consistent with these effects as maximum day-time temperature represents the point at which heat accumulation in the lower atmosphere peaks, while daily minimum temperatures corresponds to the point where the accumulated heat has radiated back into the atmosphere. As a result, reduced solar absorption due to clouds also reduces the accumulation of non-latent energy into the lower atmosphere (Doan et al., 2022), resulting in a lower DTR (see Equation 6). The dependency of longwave optical thickness on DTR arises by invoking the maximum power limit on vertical turbulent exchange (Ghausi et al., 2023; Kleidon & Renner, 2013). The increased longwave optical thickness of the atmosphere leads to an enhanced radiative heating of the surface which increases the energy available to evaporate water and results in a reduced heat accumulation in the lower atmosphere. These results highlight the strong control of radiation on DTR.

To further examine the variability around the mean in Figures 2a and 2c, we decompose the response of DTR to clear-sky fraction by stratifying the data according to different surface water availability conditions. The data were then stratified into three cases of water availability: $f_w < 0.2$, $f_w = (0.2–0.8)$ and $f_w > 0.8$. f_w is calculated as the ratio of actual to potential evaporation. These cases were chosen to roughly correspond to the three evaporative regimes: water-limited, transitional/equitant and energy-limited, respectively (Koster et al., 2009; McVicar et al., 2012; Seneviratne et al., 2010).

We found a clear distinction in the decomposed responses with dry conditions responding more strongly to changes in clear-sky fraction than wet conditions. Variability in the response of DTR to changes in cloud cover was largely explained by changes in surface water availability. Similar results were obtained when the analysis was repeated at a single site (Figure S8 in Supporting Information S1). The predicted stronger response of DTR to

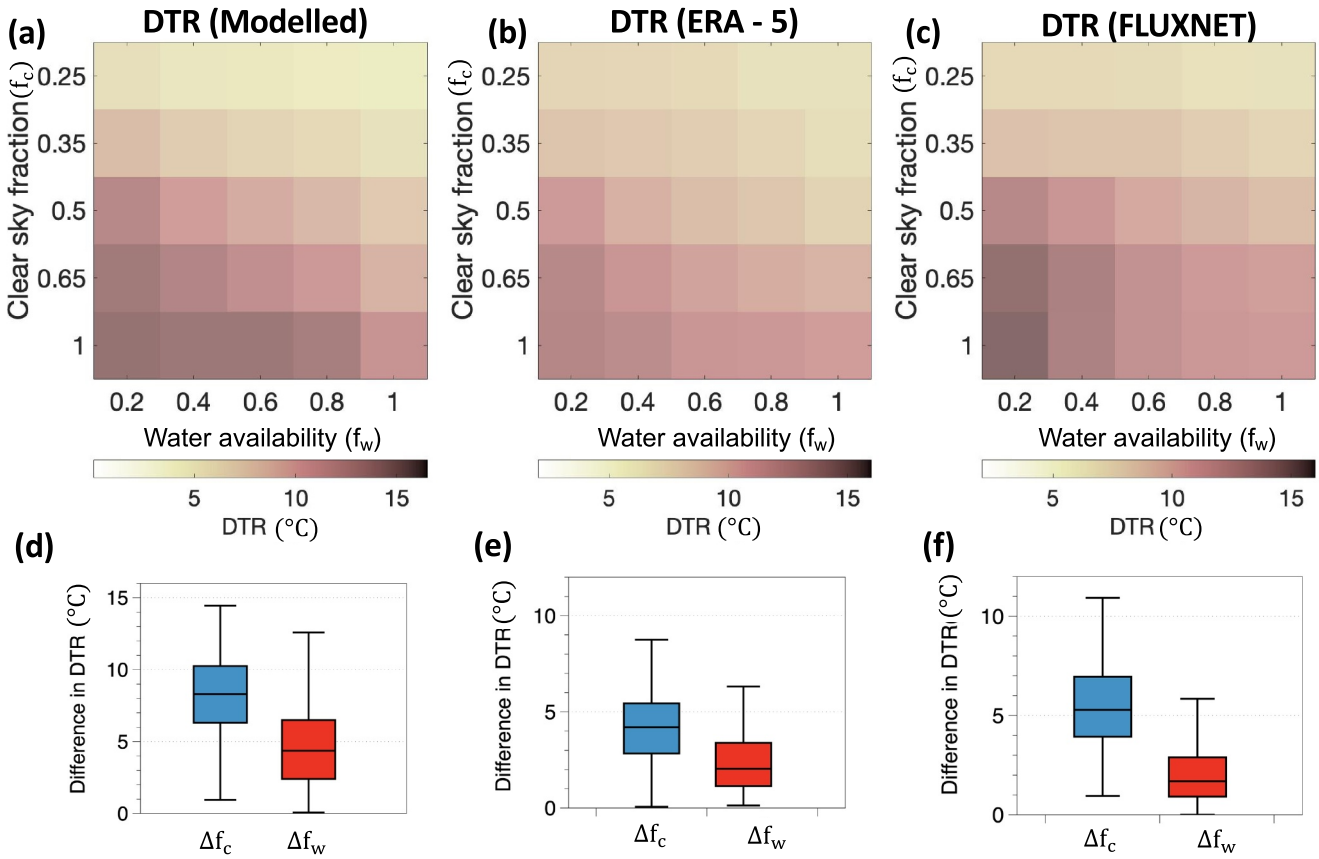

Figure 3. (a) Variation of estimated diurnal air temperature range (DTR) over the phase space defined by different surface water availability (f_w) along the *x*-axis and clear-sky fraction (f_c) along the *y*-axis. (b–c) same as (a), but for ERA5 and FLUXNET observations respectively. (d) Isolating the difference in DTR with clear-sky fraction alone Δf_c (blue) and surface water availability alone Δf_c (red), (e–f) same as (d) but for ERA5 data and FLUXNET observations respectively. Boxplot elements are as described in Figure 1.

clouds during drier conditions is supported by both FLUXNET and ERA5 data sets (Figures 2d–2f) and is in line with findings reported previously (Dai et al., 1999). Our approach provides a physical explanation for this response, as the increase in evaporation during wet conditions decreases the non-latent energy input in the boundary layer, thereby dampening the direct response of DTR on solar radiation.

4.2. Daily DTR Responses to Cloud Cover and Surface Water Availability

To quantify the effect of clouds and surface water availability on DTR, we created a two-dimensional "phase space" characterized by the different cloud-cover conditions using clear-sky fraction (f_c) and different surface water conditions using the water-availability factor (f_w) respectively. Each day was then positioned within this two-dimensional space with its DTR based on the daily values of f_c and f_w. Figures 3a–3c show these plots for the estimated DTR values, ERA5 reanalysis and FLUXNET observations, respectively. We find a clear and consistent pattern such that both, increases in cloudiness and surface water-availability reduce DTR (McVicar & Jupp, 1999). The highest DTR values were observed on predominantly dry and clear-sky days. This is consistent with the reported potential risk of extremes in DTR with compound dry and hot extremes induced by precipitation deficits (He et al., 2015). On the other hand, the lowest DTR values were observed on the cloudiest and wettest days (McVicar & Jupp, 1999). Similar phase-space patterns in DTR were obtained when the analysis was repeated at individual sites (Figure S10 in Supporting Information S1).

Next, we calculated the temperature gradients in this phase space for each site, thus isolating the changes in DTR caused solely by changes in clear-sky fraction (Δf_c) and water availability (Δf_w). These are depicted as box plots in Figures 3d–3f. We find that the reduction in DTR by cloudiness was nearly twice as pronounced as the reduction attributable to changes in surface water availability. These patterns estimated by our approach were

consistent with FLUXNET and ERA5 data sets (Figure 3). However, our approach tends to overestimate the mean reduction in DTR to changes in surface water availability (Figure 3d). This can be attributed to two primary assumptions in our approach. First, we assume a constant boundary layer height during both wet and dry conditions, while observations show an increased height with drier conditions (Denissen et al., 2021). The increased growth of the boundary layer during dry conditions increases the heat storage capacity and can partly compensate for the increase in DTR (Doan et al., 2022; Panwar et al., 2019). The sensitivity analysis of modeled DTR showed that increasing the boundary layer height from 1,000 m to 2,000 m can reduce DTR by approximately 2–3°C (Figure S17 in Supporting Information S1). Not accounting for this change overestimates the DTR response to surface water-stress by roughly the same magnitude (Figures 3d–3f). Secondly, we assume that the heat storage is zero across the whole diurnal cycle and there is no memory of prior conditions. The violation of this assumption can make DTR overly sensitive to changes in antecedent radiative and surface water availability conditions. While these assumptions may cause some discrepancies in terms of magnitude of changes, our approach still provides a strong physical foundation to explain the direction of these changes. Both of these assumptions could be dynamically modeled in future research.

It is important to note that changes in DTR with surface water availability do not imply that decreases in evaporation always reduce DTR. This happens only in the "water-limited" evaporative regime where surface water availability directly affects evaporation rates and land-atmosphere coupling is strongest (Seneviratne et al., 2010). Over wet periods in which evaporation is limited by energy, the DTR increases with evaporation because of increases in solar radiation and radiative heating at the surface (Figure S11 in Supporting Information S1).

Our findings reveal that day-to-day variations in DTR are shaped by radiative effects mainly by the heating of solar radiation but also modulated by surface water availability over land that control evaporation. The strong dependence of DTR on solar radiation has already been widely reported by previous studies. Owing to this, the DTR has also been used as a proxy for atmospheric transmittance (Bristow & Campbell, 1984) and surface solar radiation (Makowski et al., 2009). Our approach provides a parsimonious physical mechanism that explains this relation, and further explains the reported weak sensitivity of DTR to radiation during wet conditions (Dai et al., 1999).

Our approach shows that DTR contains imprints of surface evaporative conditions as the water availability at the surface directly affects the energy input into the lower atmosphere. This implies that information on surface water limitation is included in observations of the diurnal temperature range. It may be possible to exploit this relation to infer water limitation and evaporation rates directly from widely observable temperature observations without accounting for additional parameterization to represent surface water limitation. This interpretation is consistent with recent approaches that only use near-surface meteorological observations to estimate evaporation rates (McColl et al., 2019; McColl & Rigden, 2020).

4.3. DTR Responses to Changes in Greenhouse Gas Forcing

We then apply our approach to estimate multi-decadal changes in DTR in response to changes in radiative forcing driven by increasing greenhouse gas concentrations that enhance downward longwave radiation, while assuming no changes in solar radiation and evaporative fraction. We use the longwave optical thickness of the atmosphere (τ) as a proxy to represent these changes. The sensitivity of DTR to changes in daily mean temperature (T) were then calculated by using the sensitivity of DTR to changes in τ and the sensitivity of temperature to changes in τ as described by:

$$\frac{d(\mathrm{DTR})}{dT} = \frac{d(\mathrm{DTR})}{d\tau} \cdot \left(\frac{dT}{d\tau}\right)^{-1} \tag{7}$$

The first term $d(\mathrm{DTR})/d\tau$ was estimated by differentiating Equation 6 and then comparing it with observed responses from FLUXNET and ERA5 (Figure 4a). We find that DTR reduces as the longwave optical thickness of the atmosphere increases. This is also expected as an optically thicker atmosphere will increase minimum temperatures by reducing longwave radiative cooling at night and thereby reduce DTR (A. Betts, 2006). The second term, $dT/d\tau$, was taken from Kleidon and Renner (2017), who show that an increase in optical depth $\Delta\tau = 0.18$ yields a global surface warming of 5.0 K and a downwelling longwave increase of 33 W m^{-2},

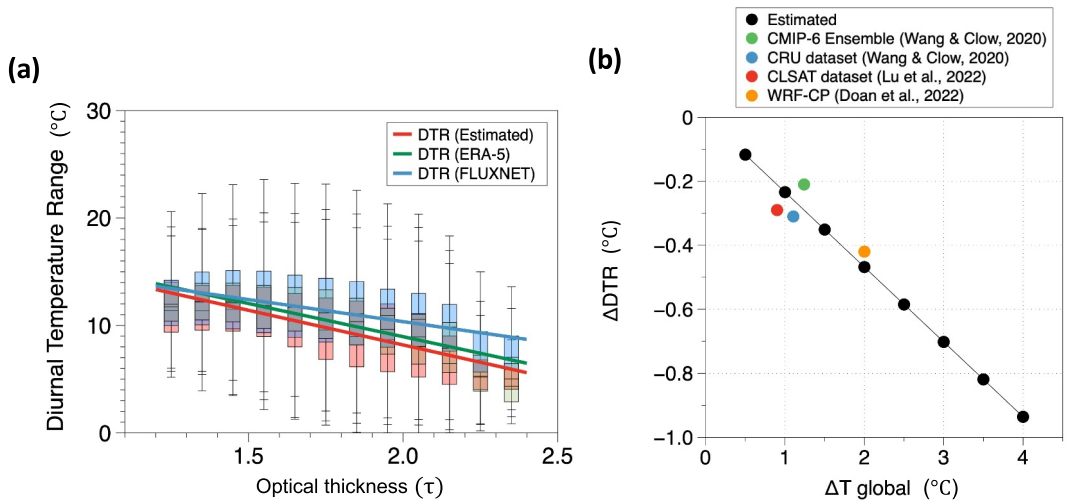

Figure 4. (a) Variation of the diurnal air temperature range (DTR) with the longwave optical thickness of the atmosphere for estimated values (red), ERA5 data (green), and FLUXNET observations (blue). (b) Changes in DTR with an increase in mean temperature. Black (dots and line) denote the sensitivity estimated by our approach. Colored dots are the estimates derived from other studies as indicated in the legend. Boxplot elements are as described in Figure 1.

consistent with CMIP5 4 × CO_2 simulations (warming 2.9–6.0 K; downwelling longwave radiation increase 20–42 W m^{-2}; their Figure S1 in Supporting Information S1).

Equation 7 then yields a reduction in DTR by 0.23°C for every 1°C increase in mean temperature. This is shown as a black solid line in Figure 4b. This estimate closely aligns with the colored dots presented in Figure 4b, which represent estimates derived from different studies using climate model simulations and observation-based data sets (Doan et al., 2022; Lu et al., 2022; K. Wang & Clow, 2020). While this response does not need to be linear, the close agreement of our estimate with observations shows that changes in greenhouse gas forcing alone can, to a first order, explain the observed decline in DTR.

Our estimate is based on an increase in longwave optical thickness as a result of increased greenhouse gas forcing alone. While this change includes the water-vapor feedback, we purposely neglect any changes to hydrologic cycling. As a result, changes in cloud-cover and surface water availability were assumed to be unaffected by the warming. The dependence of equilibrium evaporative fraction (f_{eq}) on temperature is also neglected. While all of these effects can also be diagnosed using Equation 6, the agreement of our estimate in Figure 4b implies that changes in greenhouse gas forcing alone is sufficient to explain the observed decline in DTR without explicitly accounting for changes in hydrologic cycling. It can be seen from Equation 6 that both the increase in f_{eq} and cloud-cover will reduce DTR. This implies that if the hydrologic cycle intensifies with warming (Held & Soden, 2006; Kleidon & Renner, 2013), this could further reduce DTR. On the other hand, decadal variations in solar-radiation, decreases in aerosol concentration and/or reductions in cloud-cover can increase the DTR. While such an increase has already been reported by recent studies (Huang et al., 2023; Zhong et al., 2023), it can also be tested and diagnosed using our approach.

We also note that increasing the optical thickness of a gray atmosphere can result in a much greater temperature increase compared with increasing CO_2 in a spectrally-resolved atmosphere. This is due to the effect of atmospheric windows that allow radiation to escape to space (Costa & Shine, 2012). This can be improved by including a more detailed representation of radiative transfer. Despite these assumptions, we demonstrate that our approach parsimoniously diagnoses changes in DTR in response to increasing greenhouse gas concentrations.

The goal of our approach is to contribute to a hierarchy of models with varying complexity, aiming to identify the key physical drivers behind day-to-day variations in DTR rather than achieving higher prediction accuracy. There are residuals in our approach that are partly attributable to neglected factors like changes in ground heat flux (G) (Figures S12 and S16 in Supporting Information S1), advection effects and the assumption of a fixed boundary layer height (Figure S17 in Supporting Information S1). The effect of moisture advection and heat transport has not been directly accounted for here, but these are partly reflected in the observations of local radiative forcings

(Ghausi et al., 2023; Tian, Ghausi, et al., 2023; Tian, Zhong, et al., 2023). Our sensitivity analyses show that changes in daytime ground heat flux (0–100 W m^{-2}) reduce DTR by up to 3–4°C (Figure S16 in Supporting Information S1), while seasonal changes in daily-averaged G have smaller effects on DTR (around 1°C). Similarly, varying boundary layer height from 1,000 to 2,000 m reduces DTR by 2–3°C (Figure S17 in Supporting Information S1). Notably, these changes in DTR fall within the model's RMSE range of 3–4°C, accounting for 15%–20% of unexplained variability (Figure 1). These uncertainties are smaller than the model's ability to reproduce observed DTR responses to changes in cloud cover and surface water availability (Figures 2 and 3). This suggests that, while incorporating G or dynamic boundary layer height may improve the accuracy of our estmates, our model effectively captures the predominant controls on DTR.

Additionally, we applied the thermodynamic constraint of maximum power on the vertical surface-atmosphere exchange. This constraint enables us to derive the final expression of DTR that depends on observable atmospheric and surface forcings alone and remove the dependence from surface temperatures. This helps in the interpretation of results by avoiding any confounding variables and information on surface-energy partitioning which may not be available at most meteorological stations. However, our results are not critically dependent on the assumption of maximum power. We also show that all our results still hold if we don't explicitly account for the thermodynamic constraint (Figures S13–S15 in Supporting Information S1). These results were then produced by using net radiation diagnosed from the surface energy balance as a proxy for turbulent fluxes (Text S3 in Supporting Information S1).

To summarize, we demonstrate that changes in DTR are primarily shaped by variations in non-latent energy input to the atmospheric boundary layer, which is controlled by the partitioning of incoming solar radiation at the surface between heating the lower atmosphere and evaporation. Our findings reveal that while radiative heating and cloud effects dominate DTR variability, surface water limitation introduces a water-stress imprint on DTR, which can be used as an indicator of evaporative stress. Conversely, relying solely on DTR as a radiation proxy (Hargreaves et al., 1985), will overestimate radiative impacts under dry conditions; our model offers a means to correct this bias by decomposing observed DTR changes into radiative and evaporative components.

Furthermore, our theory reproduces the reduction in DTR with increasing mean temperatures by accounting for changes in long-term greenhouse gas forcings, implying that the first-order decline in DTR with global warming can be explained by increases in greenhouse gas forcings alone. Our approach can then be further extended to understand changes in DTR with respect to changes in vegetation, deforestation, aerosols, and other aspects of global change.

5. Conclusion

We present a simple, physically based model that link the DTR to variations in radiative fluxes and surface water availability through heat storage changes in the lower atmosphere. This model correctly explains the day-to-day variation in DTR, its response to changes in cloud-cover and surface water limitation, and its long-term (multi-decadal) response to changes in greenhouse gas forcing. By isolating radiation and surface water limitation effects, the model permits parsimonious interpretation of past and future DTR changes.

Data Availability Statement

All the data sets used in this study are freely available. FLUXNET-2015 data set is accessible from G. Pastorello et al., 2020. NASA-CERES data is accessible from NASA/LARC/SD/ASDC (2019). ERA5 land hourly data is accessible from J. Muñoz Sabater (2019). No new data was generated in our study.

Acknowledgments
We thank three anonymous reviewers and the editor for the constructive feedback. We thank the PIs of FLUXNET sites used in our analysis and the Copernicus Climate Change Service for granting access to the ERA5 reanalysis data. S.A.G., E.Z., and A.K. acknowledge financial support from the Volkswagen Stiftung through the ViTamins project. S.A.G and A.K acknowledge funding from the Max Planck Institute for Biogeochemistry, Jena-Germany. Open Access funding enabled and organized by Projekt DEAL.

References

Betts, A. K. (2006). Radiative scaling of the nocturnal boundary layer and the diurnal temperature range. *Journal of Geophysical Research*, *111*(D7), D07105. https://doi.org/10.1029/2005JD006560

Betts, A. K., Desjardins, R., & Worth, D. (2013). Cloud radiative forcing of the diurnal cycle climate of the Canadian Prairies. *Journal of Geophysical Research: Atmospheres*, *118*(16), 8935–8953. https://doi.org/10.1002/jgrd.50593

Braganza, K., Karoly, D. J., & Arblaster, J. (2004). Diurnal temperature range as an index of global climate change during the twentieth century. *Geophysical Research Letters*, *31*(13), L13217. https://doi.org/10.1029/2004GL019998

Bristow, K. L., & Campbell, G. S. (1984). On the relationship between incoming solar radiation and daily maximum and minimum temperature. *Agricultural and Forest Meteorology*, *31*(2), 159–166. https://doi.org/10.1016/0168-1923(84)90017-0

Conte, L., Renner, M., Brando, P., Oliveira dos Santos, C., Silvério, D., Kolle, O., et al. (2019). Effects of tropical deforestation on surface energy balance partitioning in southeastern Amazonia estimated from maximum convective power. *Geophysical Research Letters*, *46*(8), 4396–4403. https://doi.org/10.1029/2018GL081625

Costa, S. M. S., & Shine, K. P. (2012). Outgoing longwave radiation due to directly transmitted surface emission. *Journal of the Atmospheric Sciences*, *69*(6), 1865–1870. https://doi.org/10.1175/JAS-D-11-0248.1

Dai, A., Trenberth, K. E., & Karl, T. R. (1999). Effects of clouds, soil moisture, precipitation, and water vapor on diurnal temperature range. *Journal of Climate*, *12*(8), 2451–2473. https://doi.org/10.1175/1520-0442(1999)012<2451:EOCSMP>2.0.CO;2

Denissen, J. M. C., Orth, R., Wouters, H., Miralles, D. G., van Heerwaarden, C. C., de Arellano, J. V. G., & Teuling, A. J. (2021). Soil moisture signature in global weather balloon soundings. *npj Clim Atmos Sci*, *4*(1), 13. https://doi.org/10.1038/s41612-021-00167-w

Dhara, C. (2017). First order controls on the steady state surface energy partitioning and its sensitivity using idealized models. *(Doctoral dissertation, Staats-und Universitätsbibliothek Hamburg Carl von Ossietzky)*. Retrieved from https://ediss.sub.uni-hamburg.de/handle/ediss/7161

Dhara, C., Renner, M., & Kleidon, A. (2016). Broad climatological variation of surface energy balance partitioning across land and ocean predicted from the maximum power limit. *Geophysical Research Letters*, *43*(14), 7686–7693. https://doi.org/10.1002/2016GL070323

Doan, Q. V., Chen, F., Asano, Y., Gu, Y., Nishi, A., Kusaka, H., & Niyogi, D. (2022). Causes for asymmetric warming of sub-diurnal temperature responding to global warming. *Geophysical Research Letters*, *49*(20), e2022GL100029. https://doi.org/10.1029/2022GL100029

Easterling, D. R., Horton, B., Jones, P. D., Peterson, T. C., Karl, T. R., Parker, D. E., et al. (1997). Maximum and minimum temperature trends for the globe. *Science*, *277*(5324), 364–367. https://doi.org/10.1126/science.277.5324.364

Ghausi, S. A., Tian, Y., Zehe, E., & Kleidon, A. (2023). Radiative controls by clouds and thermodynamics shape surface temperatures and turbulent fluxes over land. *Proceedings of the National Academy of Sciences*, *120*(29), e2220400120. https://doi.org/10.1073/pnas.2220400120

Goody, R. M., & Yung, Y. L. (1989). *Atmospheric radiation: Theoretical basis* (2nd ed.). Oxford University Press. https://doi.org/10.1093/oso/9780195051346.001.0001

Hargreaves, G. L., Hargreaves, G. H., & Paul Riley, J. (1985). Irrigation water requirements for Senegal river basin. *Journal of Irrigation and Drainage Engineering*, *111*(3), 265–275. https://doi.org/10.1061/(ASCE)0733-9437(1985)111:3(265)

He, B., Huang, L., & Wang, Q. (2015). Precipitation deficits increase high diurnal temperature range extremes. *Scientific Reports*, *5*(1), 12004. https://doi.org/10.1038/srep12004

Held, I. M. (2005). The gap between simulation and understanding in climate modeling. *Bulletin of the American Meteorological Society*, *86*(11), 1609–1614. https://doi.org/10.1175/BAMS-86-11-1609

Held, I. M., & Soden, B. J. (2006). Robust responses of the hydrological cycle to global warming. *Journal of Climate*, *19*(21), 5686–5699. https://doi.org/10.1175/JCLI3990.1

Huang, X., Dunn, R. J., Li, L. Z., McVicar, T. R., Azorin-Molina, C., & Zeng, Z. (2023). Increasing global terrestrial diurnal temperature range for 1980–2021. *Geophysical Research Letters*, *50*(11), e2023GL103503. https://doi.org/10.1029/2023GL103503

Huang, Y., Dickinson, R. E., & Chameides, W. L. (2006). Impact of aerosol indirect effect on surface temperature over East Asia. *Proceedings of the National Academy of Sciences*, *103*(12), 4371–4376. https://doi.org/10.1073/pnas.0504428103

IPCC. (2021). In V. Masson-Delmotte, P. Zhai, A. Pirani, S. L. Connors, C. Péan, et al. (Eds.), *Climate change 2021: The physical science basis. Contribution of working group I to the sixth assessment report of the intergovernmental panel on climate change*. Cambridge University Press. In press. https://doi.org/10.1017/9781009157896

Karl, T. R., Kukla, G., Razuvayev, V. N., Changery, M. J., Quayle, R. G., Heim, R. R., et al. (1991). Global warming: Evidence for asymmetric diurnal temperature change. *Geophysical Research Letters*, *18*(12), 182253–182256. https://doi.org/10.1029/91GL02900

Kato, S., Rose, F. G., Rutan, D. A., Thorsen, T. J., Loeb, N. G., Doelling, D. R., et al. (2018). Surface irradiances of edition 4.0 clouds and the Earth's radiant energy system (CERES) energy balanced and filled (EBAF) data product. *Journal of Climate*, *31*(11), 4501–4527. https://doi.org/10.1175/JCLI-D-17-0523.1

Kleidon, A., & Renner, M. (2013). Thermodynamic limits of hydrologic cycling within the Earth system: Concepts, estimates, and implications. *Hydrology and Earth System Sciences*, *17*(7), 2873–2892. https://doi.org/10.5194/hess-17-2873-2013

Kleidon, A., & Renner, M. (2017). An explanation for the different climate sensitivities of land and ocean surfaces based on the diurnal cycle. *Earth System Dynamics*, *8*(3), 849–864. https://doi.org/10.5194/esd-8-849-2017

Kleidon, A., & Renner, M. (2018). Diurnal land surface energy balance partitioning estimated from the thermodynamic limit of a cold heat engine. *Earth System Dynamics*, *9*(3), 1127–1140. https://doi.org/10.5194/esd-9-1127-2018

Koster, R. D., Schubert, S. D., & Suarez, M. J. (2009). Analyzing the concurrence of meteorological droughts and warm periods, with implications for the determination of evaporative regime. *Journal of Climate*, *22*(12), 3331–3341. https://doi.org/10.1175/2008JCLI2718.1

Lei, L., Bao, J., Guo, Y., Wang, Q., Peng, J., & Huang, C. (2020). Effects of diurnal temperature range on first-ever strokes in different seasons: A time-series study in Shenzhen, China. *BMJ Open*, *10*(11), e033571. https://doi.org/10.1136/bmjopen-2019-033571

Lewis, S. C., & Karoly, D. J. (2013). Evaluation of historical diurnal temperature range trends in CMIP5 models. *Journal of Climate*, *26*(22), 9077–9089. https://doi.org/10.1175/JCLI-D-13-00032.1

Lobell, D. B. (2007). Changes in diurnal temperature range and national cereal yields. *Agricultural and Forest Meteorology*, *145*(3–4), 229–238. https://doi.org/10.1016/j.agrformet.2007.05.002

Loeb, N. G., Doelling, D. R., Wang, H., Su, W., Nguyen, C., Corbett, J. G., et al. (2018). Clouds and the Earth's radiant energy system (CERES) energy balanced and filled (EBAF) top-of-atmosphere (TOA) Edition-4.0 data product. *Journal of Climate*, *31*(2), 895–918. https://doi.org/10.1175/JCLI-D-17-0208.1

Lorenz, R. D., & McKay, C. P. (2003). A simple expression for vertical convective fluxes in planetary atmospheres. *Icarus*, *165*(2), 407–413. https://doi.org/10.1016/S0019-1035(03)00205-7

Lu, C., Sun, Y., & Zhang, X. (2022). Anthropogenic influence on the diurnal temperature range since 1901. *Journal of Climate*, *35*(22), 7183–7198. https://doi.org/10.1175/JCLI-D-21-0928.1

Makowski, K., Jaeger, E. B., Chiacchio, M., Wild, M., Ewen, T., & Ohmura, A. (2009). On the relationship between diurnal temperature range and surface solar radiation in Europe. *Journal of Geophysical Research*, *114*(D10), D00D07. https://doi.org/10.1029/2008JD011104

McColl, K. A., & Rigden, A. J. (2020). Emergent simplicity of Continental evapotranspiration. *Geophysical Research Letters*, *47*(6), e2020GL087101. https://doi.org/10.1029/2020GL087101

McColl, K. A., Salvucci, G. D., & Gentine, P. (2019). Surface flux equilibrium theory explains an empirical estimate of water-limited daily evapotranspiration. *Journal of Advances in Modeling Earth Systems*, *11*(7), 2036–2049. https://doi.org/10.1029/2019ms001685

McVicar, T. R., & Jupp, D. L. (1999). Estimating one-time-of-day meteorological data from standard daily data as inputs to thermal remote sensing based energy balance models. *Agricultural and Forest Meteorology*, *96*(4), 219–238. https://doi.org/10.1016/S0168-1923(99)00052-0

McVicar, T. R., Roderick, M. L., Donohue, R. J., & Van Niel, T. G. (2012). Less bluster ahead? Ecohydrological implications of global trends of terrestrial near-surface wind speeds. *Ecohydrology*, *5*(4), 381–388. https://doi.org/10.1002/eco.1298

Mearns, L. O., Giorgi, F., McDaniel, L., & Shields, C. (1995). Analysis of variability and diurnal range of daily temperature in a nested regional climate model: Comparison with observations and doubled CO2 results. *Climate Dynamics*, *11*(4), 193–209. https://doi.org/10.1007/BF00215007

Muñoz Sabater, J. (2019). ERA5-Land hourly data from 1950 to present. *Copernicus Climate Change Service (C3S) Climate Data Store (CDS)*. https://doi.org/10.24381/cds.e2161bac

NASA/LARC/SD/ASDC. (2019). CERES energy balanced and filled (EBAF) TOA and surface monthly means data in netCDF edition 4.1 [Dataset]. *NASA Langley Atmospheric Science Data Center DAAC*. https://doi.org/10.5067/TERRA-AQUA/CERES/EBAF_L3B.004.1

Panwar, A., & Kleidon, A. (2022). Evaluating the response of diurnal variations in surface and air temperature to evaporative conditions across vegetation types in FLUXNET and ERA5. *Journal of Climate*, *35*(19), 6301–6328. https://doi.org/10.1175/JCLI-D-21-0345.1

Panwar, A., Kleidon, A., & Renner, M. (2019). Do surface and air temperatures contain similar imprints of evaporative conditions? *Geophysical Research Letters*, *46*(7), 3802–3809. https://doi.org/10.1029/2019GL082248

Pastorello, G., Trotta, C., Canfora, E., Chu, H., Christianson, D., Cheah, Y. W., et al. (2020). The FLUXNET2015 dataset and the ONEFlux processing pipeline for eddy covariance data. *Scientific Data*, *7*(1), 225. https://doi.org/10.1038/s41597-020-0534-3

Priestley, C. H. B., & Taylor, R. J. (1972). On the assessment of surface heat flux and evaporation using large-scale parameters. *Monthly Weather Review*, *100*(2), 81–92. https://doi.org/10.1175/1520-0493(1972)100%3C0081:OTAOSH%3E2.3.CO;2

Reichstein, M., Falge, E., Baldocchi, D., Papale, D., Aubinet, M., Berbigier, P., et al. (2005). On the separation of net ecosystem exchange into assimilation and ecosystem respiration: Review and improved algorithm. *Global Change Biology*, *11*(9), 1424–1439. https://doi.org/10.1111/j.1365-2486.2005.001002.x

Renner, M., Wild, M., Schwarz, M., & Kleidon, A. (2019). Estimating shortwave clear-sky fluxes from hourly global radiation records by quantile regression. *Earth and Space Science*, *6*(8), 1532–1546. https://doi.org/10.1029/2019EA000686

Seneviratne, S. I., Corti, T., Davin, E. L., Hirschi, M., Jaeger, E. B., Lehner, I., et al. (2010). Investigating soil moisture-climate interactions in a changing climate: A review. *Earth-Science Reviews*, *99*(3–4), 125–161. https://doi.org/10.1016/j.earscirev.2010.02.004

Slatyer, R. O., & McIlroy, I. C. (1961). *Practical micrometeorology*. CSIRO.310.

Stone, D., & Weaver, A. (2003). Factors contributing to diurnal temperature range trends in twentieth and twenty-first century simulations of the CCCma coupled model. *Climate Dynamics*, *20*(5), 435–445. https://doi.org/10.1007/s00382-002-0288-y

Stull, R. (2017). *Practical meteorology: An Algebra-based survey of atmospheric science -version 1.02b*. University of British Columbia. pages. isbn 978-0-88865-283-6.940.

Sun, X., Ren, G., You, Q., Ren, Y., Xu, W., Xue, X., et al. (2018). Global diurnal temperature range (DTR) changes since 1901. *Climate Dynamics*, *52*(5), 3343–3356. https://doi.org/10.1007/s00382-018-4329-6

Tian, Y., Ghausi, S. A., Zhang, Y., Zhang, M., Xie, D., Cao, Y., et al. (2023). Radiation as the dominant cause of high-temperature extremes on the eastern Tibetan Plateau. *Environmental Research Letters*, *18*(7), 074007. https://doi.org/10.1088/1748-9326/acd805

Tian, Y., Zhong, D., Ghausi, S. A., Wang, G., & Kleidon, A. (2023). Understanding variations in downwelling longwave radiation using Brutsaert's equation. *Earth System Dynamics*, *14*(6), 1363–1374. https://doi.org/10.5194/esd-14-1363-2023

Wang, J., & Liu, D. (2023). Larger diurnal temperature range undermined later autumn leaf senescence with warming in Europe. *Global Ecology and Biogeography*, *32*(5), 734–746. https://doi.org/10.1111/geb.13674

Wang, K., & Clow, G. D. (2020). The diurnal temperature range in CMIP6 models: Climatology, variability, and evolution. *Journal of Climate*, *33*(19), 8261–8279. https://doi.org/10.1175/JCLI-D-19-0897.1

Wild, M., Gilgen, H., Roesch, A., Ohmura, A., Long, C. N., Dutton, E. G., et al. (2005). From dimming to brightening: Decadal changes in solar radiation at earth's surface. *Science*, *308*(5723), 847–850. https://doi.org/10.1126/science.1103215

Yang, J., Liu, H. Z., Ou, C. Q., Lin, G. Z., Zhou, Q., Shen, G. C., et al. (2013). Global climate change: Impact of diurnal temperature range on mortality in Guangzhou, China. *Environmental Pollution*, *175*, 131–136. https://doi.org/10.1016/j.envpol.2012.12.021

Zhong, Z., He, B., Chen, H. W., Chen, D., Zhou, T., Dong, W., et al. (2023). Reversed asymmetric warming of sub-diurnal temperature over land during recent decades. *Nature Communications*, *14*(1), 7189. https://doi.org/10.1038/s41467-023-43007-6

Zhou, L., Dickinson, R. E., Tian, Y., Fang, J., Li, Q., Kaufmann, R. K., et al. (2004). Evidence for a significant urbanization effect on climate in China. *Proceedings of the National Academy of Sciences*, *101*(26), 9540–9544. https://doi.org/10.1073/pnas.0400357101

Zhou, L., Dickinson, R. E., Tian, Y., Vose, R. S., & Dai, Y. (2007). Impact of vegetation removal and soil aridation on diurnal temperature range in a semiarid region: Application to the Sahel. *Proceedings of the National Academy of Sciences USA*, *104*(46), 17937–17942. https://doi.org/10.1073/pnas.0700290104